




OPEN ACCESS

Original research

# CRIP1 fosters MDSC trafficking and resets tumour microenvironment via facilitating NF- $\kappa$ B/p65 nuclear translocation in pancreatic ductal adenocarcinoma

Xiaomeng Liu,<sup>1,2,3,4</sup> Rong Tang,<sup>1,2,3,4</sup> Jin Xu,<sup>1,2,3,4</sup> Zhen Tan,<sup>5</sup> Chen Liang,<sup>1,2,3,4</sup> Qingcai Meng,<sup>1,2,3,4</sup> Yubin Lei,<sup>6</sup> Jie Hua,<sup>1,2,3,4</sup> Yiyin Zhang,<sup>7</sup> Jiang Liu,<sup>1,2,3,4</sup> Bo Zhang,<sup>1,2,3,4</sup> Wei Wang,<sup>1,2,3,4</sup> Xianjun Yu,<sup>1,2,3,4</sup> Si Shi <sup>1,2,3,4</sup>

► Additional supplemental material is published online only. To view, please visit the journal online (<http://dx.doi.org/10.1136/gutjnl-2022-329349>).

For numbered affiliations see end of article.

## Correspondence to

Associate Professor Si Shi, Shanghai Pancreatic Cancer Institute, Shanghai 200032, China; [shisi@fudanpci.org](mailto:shisi@fudanpci.org) and Professor Xianjun Yu, Department of Pancreatic Surgery, Fudan University Shanghai Cancer Center, Shanghai 200032, China; [yuxianjun@fudan.edu.cn](mailto:yuxianjun@fudan.edu.cn)

XL, RT and JX contributed equally.

Received 19 December 2022  
Accepted 23 July 2023  
Published Online First 4 August 2023

## ABSTRACT

**Objective** Pancreatic ductal adenocarcinoma (PDAC) is among the most immunosuppressive tumour types. The tumour immune microenvironment (TIME) is largely driven by interactions between immune cells and heterogeneous tumour cells. Here, we aimed to investigate the mechanism of tumour cells in TIME formation and provide potential combination treatment strategies for PDAC patients based on genotypic heterogeneity.

**Design** Highly multiplexed imaging mass cytometry, RNA sequencing, mass cytometry by time of flight and multiplex immunofluorescence staining were performed to identify the pro-oncogenic proteins associated with low immune activation in PDAC. An in vitro coculture system, an orthotopic PDAC allograft tumour model, flow cytometry and immunohistochemistry were used to explore the biological functions of cysteine-rich intestinal protein 1 (CRIP1) in tumour progression and TIME formation. RNA sequencing, mass spectrometry and chromatin immunoprecipitation were subsequently conducted to investigate the underlying mechanisms of CRIP1.

**Results** Our results showed that CRIP1 was frequently upregulated in PDAC tissues with low immune activation. Elevated CRIP1 expression induced high levels of myeloid-derived suppressor cell (MDSC) infiltration and fostered an immunosuppressive tumour microenvironment. Mechanistically, we primarily showed that CRIP1 bound to nuclear factor kappa-B (NF- $\kappa$ B)/p65 and facilitated its nuclear translocation in an importin-dependent manner, leading to the transcriptional activation of CXCL1/5. PDAC-derived CXCL1/5 facilitated the chemotactic migration of MDSCs to drive immunosuppression. SX-682, an inhibitor of CXCR1/2, blocked tumour MDSC recruitment and enhanced T-cell activation. The combination of anti-PD-L1 therapy with SX-682 elicited increased CD8+T cell infiltration and potent antitumor activity in tumour-bearing mice with high CRIP1 expression.

**Conclusions** The CRIP1/NF- $\kappa$ B/CXCL axis is critical for triggering immune evasion and TIME formation in PDAC. Blockade of this signalling pathway prevents MDSC trafficking and thereby sensitises PDAC to immunotherapy.

## WHAT IS ALREADY KNOWN ON THIS TOPIC

- ⇒ Pancreatic ductal adenocarcinoma (PDAC) is one of the most lethal tumours and has an immunosuppressive microenvironment. Dynamic interactions between immune cells and other cells, especially heterogeneous cancer cells, contribute to tumour immune microenvironment (TIME) formation in PDAC.
- ⇒ Targeting myeloid-derived suppressor cells (MDSCs) in the TIME has emerged as a promising therapeutic strategy for some cancer types. The therapeutic efficacy of this approach in PDAC patients remains uncertain, although blocking MDSC recruitment has been shown to impede tumourigenesis in mouse models.
- ⇒ Immune checkpoint blockade (ICB) and multimodal immunotherapies have limited efficacy in patients with PDAC. Personalised combinations of immunotherapy strategies are required for subgroups of patients with PDAC.

## WHAT THIS STUDY ADDS

- ⇒ CRIP1 is frequently upregulated in PDAC tissues with low immune activation and predicts a poor prognosis of PDAC.
- ⇒ CRIP1 binds to NF- $\kappa$ B/p65 and facilitates its nuclear translocation in an importin-dependent manner, leading to the transcriptional activation of CXCL1/5. PDAC-derived CXCL1/5 facilitates the chemotactic migration of MDSCs to drive immunosuppression.
- ⇒ SX-682, an inhibitor of CXCR1/2, blocks tumour MDSC recruitment and increases T-cell activation. Combining anti-PD-L1 therapy with SX-682 elicits increased CD8+T cell infiltration and potent antitumour activity in tumour-bearing mice with high CRIP1 expression.

## HOW THIS STUDY MIGHT AFFECT RESEARCH, PRACTICE OR POLICY

- ⇒ CRIP1 may be an attractive novel target for improving immune activation in PDAC and may benefit patients with precise immunotherapy.
- ⇒ Strategies to block the CRIP1/NF- $\kappa$ B/CXCL axis and prevent MDSC trafficking may increase the efficacy of ICB therapy in PDAC patients with high CRIP1 expression.



© Author(s) (or their employer(s)) 2023. Re-use permitted under CC BY-NC. No commercial re-use. See rights and permissions. Published by BMJ.

**To cite:** Liu X, Tang R, Xu J, et al. *Gut* 2023;**72**:2329–2343.

## INTRODUCTION

Pancreatic ductal adenocarcinoma (PDAC) is one of the most lethal solid tumours.<sup>1</sup> More than 80% of PDAC patients experience disease relapse even after they undergo surgical resection.<sup>2</sup> Furthermore, the combination of chemotherapy and radiotherapy induces only short-lived partial remission or stable disease in newly diagnosed patients.<sup>3</sup> Recent discoveries deciphering immune landscapes have fostered the development of immunotherapies, such as immune checkpoint blockade (ICB).<sup>4,5</sup> ICB agents have transformed the outlook of advanced patients with solid tumours, including those with melanoma and lung cancer, but only a small subset of PDAC patients may benefit from it.<sup>6–8</sup>

The refractory nature of PDAC to immunotherapies is unique across human cancers.<sup>9</sup> Classically, PDAC exhibits an immunologically “cold” tumour microenvironment (TME) that is characterised by the prominent infiltration of tumour-promoting immune cells, such as myeloid-derived suppressor cells (MDSCs), and is typically devoid of CD8+T cells, resulting in the loss of cytotoxic effector functions.<sup>10,11</sup> MDSCs represent pathologically activated monocytes and relatively immature neutrophils.<sup>12</sup> Two major subsets of MDSCs, polymorphonuclear (PMN-MDSC) and monocytic (M-MDSC), have been identified and extensively studied.<sup>13</sup> How to identify these cells in the field of MDSC research is still a controversial issue. Although these two groups of cells have distinct phenotypes, they share many common features in biochemical and functional activities. Immunosuppression is the main feature of MDSCs, and the most prominent factors implicated in MDSC-mediated suppression of T cells include arginase 1 (Arg1), NO, ROS and prostaglandin E2.<sup>14,15</sup>

MDSCs have been shown to migrate to tumours due to the chemokine gradient generated by the growing tumour. The migration of MDSCs mainly relies on the expression of the chemokine receptor CXCR1/2 and its cognate ligands CXCL1, CXCL2 and CXCL5.<sup>16</sup> Blocking MDSC recruitment has been shown to impede tumourigenesis in mouse models, but the therapeutic efficacy of this approach in PDAC patients remains uncertain.<sup>17</sup> SX-682, a potent allosteric inhibitor of CXCR1/2 that blocks MDSC recruitment, has already been undergoing clinical trials in patients with PDAC (NCT04477343), but the results have not yet been disclosed. Targeting chemokines for the treatment of PDAC has been of interest for a long time. According to basic research, inhibition of CXCR4 in a PDAC mouse model resulted in a tumour response.<sup>18</sup> However, the results of related clinical trials were not all satisfactory because of the high heterogeneity of PDAC. This suggests that targeting chemokines, including SX-682, which blocks MDSC recruitment, needs to be explored in more detail in certain populations of PDAC patients.

The immunosuppressive PDAC microenvironment is driven by dynamic interactions between immune cells and a variety of cells in host tissue.<sup>19</sup> Heterogeneous tumour cells are the most important component of PDAC, and their unique genetic landscape plays an important role in programming the tumour immune landscape.<sup>20,21</sup> In addition to their classical intrinsic oncogenic effects on the fate of cancer cells, genetic alterations in PDAC cells have been shown to coordinate a paracrine network to establish a TME composed of immune cells with suppressive functions.<sup>22</sup> For instance, tumour cell-intrinsic granulocyte macrophage colony-stimulating factor and CXCL1 secretion promote MDSC infiltration and T-cell exclusion.<sup>23,24</sup> Despite the presence of a common oncogenic pathway, PDAC is a genetically

heterogeneous disease characterised by genetic and epigenetic changes and diverse clinical phenotypes.<sup>25</sup> The identification of precise immunotherapy strategies for patients based on specific PDAC genotypes and phenotypes may provide novel insights.

Cysteine-rich intestinal protein 1 (CRIP1), a member of the LIM/dual zinc-finger protein family, is aberrantly expressed in various tumour types and plays a critical role in tumour development.<sup>26–28</sup> However, the role of CRIP1 in PDAC progression and the related mechanisms have rarely been studied. Here, we aimed to identify the crucial genes associated with low immune activation in PDAC using highly multiplexed imaging mass cytometry (IMC) and RNA sequencing. Our findings primarily revealed a previously unexplored mechanism by which CRIP1 in tumour cells affects immune cells. The feasibility of targeting this mechanism to sensitise PDAC to immunotherapy was further explored. This study provides promising insights into personalised combination treatment strategies for subgroups of patients with PDAC.

## MATERIALS AND METHODS

Additional materials and methods are included in online supplemental material.

## RESULTS

### CRIP1 is a crucial pro-oncogenic protein associated with low immune activation in PDAC

To explore the microenvironment of PDAC and its formation mechanism, we performed highly multiplexed IMC and RNA sequencing to analyse tumour specimens from 40 patients with PDAC (figure 1A). Based on the IMC protocols for cancer, we established a 17-marker panel for PDAC tissues, including structural markers, such as E-cadherin and collagen, and immunological markers (figure 1B). We detected major cell types, including E-cadherin+epithelial cells and  $\alpha$ SMA+fibroblasts, and the proliferation marker Ki-67 (figure 1C). Three subsets of immune cells were detected: CD3+T cells, CD68+myeloid cells and CD20+B cells. CD8+T cells, CD4+T cells and Tregs were further identified among T cells (figure 1D). The scanned images were subjected to cell segmentation, followed by an established pipeline developed by Schapiro *et al.*<sup>29</sup> The marker expression levels in each cell in the images were quantified, and 20 cell clusters were identified using FlowSOM (online supplemental figure 1A). Based on the different expression levels of cell type-specific markers, the 20 clusters were merged into 7 populations. These populations included three clusters of cancer cells, six clusters of fibroblasts and eight clusters of immune cells (figure 1E). Neighbourhood analysis showed abundant interactions or avoidance relations among the 20 clusters, which further indicated the complex cellular communication in the PDAC microenvironment (online supplemental figure 1B). High-dimensional marker expression information was analysed using t-distributed stochastic neighbour embedding (tSNE) (online supplemental figure 1C). The distribution of these main populations and representative markers was also visualised, and the cell population distribution was consistent with that of the representative markers (figure 1F; online supplemental figure 1D). Because CD8+T cells reflect the activation of the immune microenvironment, we divided the samples into two groups based on the infiltration of CD8+T cells (online supplemental figure 1E,F). RNA sequencing was then performed to analyse tumour specimens of these two indicated groups, and upregulated differentially expressed genes (DEGs) were identified in specimens with low CD8+T cell infiltration (figure 1H).

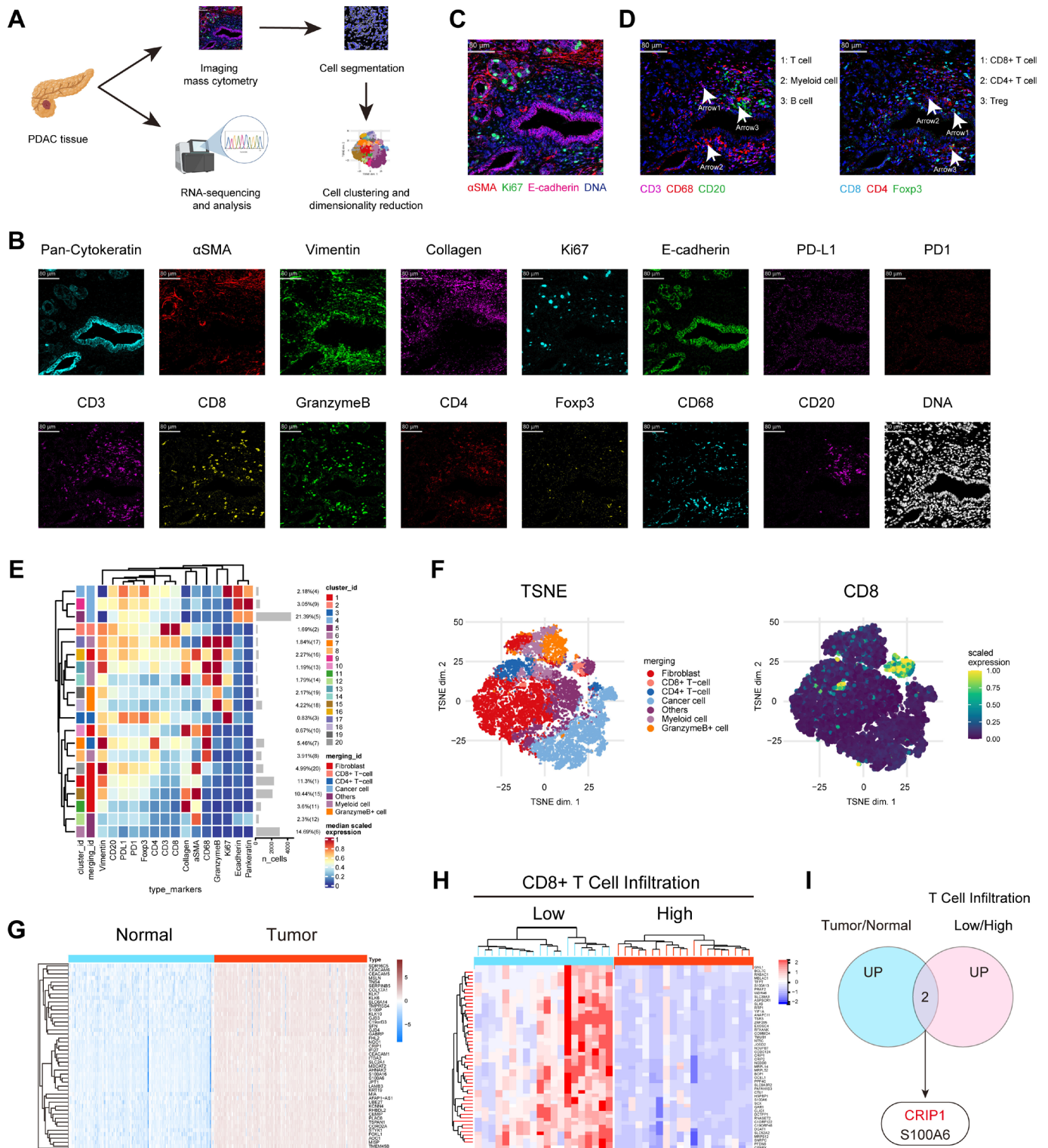


**Figure 1** CRIP1 is a crucial pro-oncogenic protein associated with low immune activation in PDAC. (A) Schematic diagram of the acquisition and analysis of data from 40 PDAC specimens. (B) Representative images of staining using antibodies against the indicated marker. (C) E-cadherin was used to distinguish epithelial cells,  $\alpha$ SMA was used to distinguish specifically fibroblasts, and Ki-67 was used to distinguish proliferating cells. (D) CD3, CD4 and CD8 were used to indicate T cells, CD68 was used to indicate myeloid cells, and CD20 was used to indicate B cells. (E) Heatmap of the median marker intensities of the 15 markers in the 7 cell populations obtained by manual merging of the 20 meta-clusters generated using FlowSOM. (F) Seven cell populations obtained by manual merging in a t-SNE plot; CD8 expression in the cells from the PDAC samples in a t-SNE plot. (G) Heatmap of the upregulated genes in PDAC tissues from the TCGA database compared with adjacent tissues from the GTEx database. Log<sub>2</sub>-fold-change >2, FDR<0.01. (H) Heatmap showing the DEGs in PDAC specimens between the CD8 high and CD8 low groups. (I) Venn diagram illustrating the overlap of upregulated genes between the tumour/normal groups and T-cell infiltration low/high groups. DEGs, differentially expressed genes; FDR, false discovery rate; PDAC, pancreatic ductal adenocarcinoma; TCGA, The Cancer Genome Atlas; t-SNE, t-distributed stochastic neighbour embedding.



Notably, cell type-specific markers, such as E-cadherin, CD8 and CD4, were not included among the DEGs. DEGs that were upregulated in PDAC compared with normal tissues from The Cancer Genome Atlas (TCGA) were also identified (figure 1G). Then, we overlapped the two sets of DEGs, and two genes were identified (figure 1I). CRIP1 was selected for further study since it has been rarely studied in PDAC.

Next, we performed an analysis of the TCGA cohort to determine the correlation of CRIP1 expression with immune cell infiltration. Unsupervised consensus clustering analysis was performed to identify three independent subclusters, and CRIP1 was associated with the immune-desert subtype of PDAC (online supplemental figure 2A–C). CRIP1 expression was negatively correlated with immune activation through analysis with different algorithms (online supplemental figure 2D,E). We further integrated two large open scRNA-seq datasets of PDAC and found that CRIP1 was significantly upregulated in ductal cells isolated from PDAC tissue compared with ductal cells from normal pancreatic tissue (online supplemental figure 3A,B). Interestingly, S100A6 expression was significantly upregulated in fibroblasts in PDAC tissue compared with normal pancreatic tissue, suggesting that unlike CRIP1 expression, S100A6 expression in fibroblasts may be associated with PDAC (online supplemental figure 3C,D). The CytoTRACE results indicated that both CRIP1 and S100A6 were upregulated in more differentiated stellate cells (online supplemental figure 4). Thus, we believe that it is very important and necessary to focus on the role of CRIP1 in PDAC cells herein. Immunofluorescence staining indicated that CRIP1 was mainly in the nucleus of PDAC cells (online supplemental figure 5A). Furthermore, CRIP1 transcription was higher in tumour tissues from patients in the Fudan University Shanghai Cancer Center (FUSCC) and open database (online supplemental figure 5B,C). CRIP1 was rarely expressed in normal pancreatic tissues but was commonly detected in ductal epithelial cells of pancreatic intraepithelial neoplasia and PDAC (online supplemental figure 5D,E). These results show that CRIP1 is expressed at high levels in PDAC and is associated with low immune activation, suggesting that CRIP1 deserves further exploration as a potential driver of the immunosuppressive PDAC microenvironment.

### CRIP1 induces high MDSC infiltration and low T-cell infiltration in the PDAC microenvironment

We processed fresh PDAC samples from 20 patients and conducted mass cytometry by time of flight (CyTOF) and bioinformatics analyses to further explore the role of CRIP1 in immunosuppression (figure 2A). We established a 15-marker panel for T cells and a 17-marker panel for non-T cells. The marker expression levels in T cells were quantified, and 20 cell clusters were identified using FlowSOM and merged into the 5 populations (figure 2B). The distributions of these clusters, populations and representative markers were visualised in a t-SNE plot (figure 2C,D; online supplemental figure 6A). The t-SNE plot showed decreased infiltration of CD8+T cells and CD4+T cells in the CRIP1 high group (figure 2E). Furthermore, expression of the exhaustion marker CD279 was increased in samples with high CRIP1 expression (figure 2F). The increase in CD279 expression was present in both CD4+T cells and CD8+T cells, which suggested extensive T-cell exhaustion in PDAC (figure 2G; online supplemental figure 6B,C). In samples with high CRIP1 expression, some CD4+T cells presented higher CD25 expression, indicating that they could be Tregs (figure 2H; online supplemental figure 6D). According to the

results in figure 2E, the CD45+CD3- cluster was significantly enriched in tumours with high CRIP1 expression, suggesting that there were great differences in non-T cell enrichment between tumour types. Next, we conducted CyTOF and t-SNE to analyse non-T cells. CD3 was used as the T cell marker to distinguish non-T-cell populations more accurately. Twenty cell clusters were identified using FlowSOM, the total cell population was divided into eight subclusters, and MDSCs were found to be significantly enriched in the CRIP1 high group (figure 2I–L; online supplemental figure 6E). Therefore, we speculate that this group of cells with great differences in figure 2E is mainly the MDSC cluster. Of course, there are likely to be many other cells involved. In the TCGA cohort, we analysed CRIP1 expression and the levels of infiltrating immune cells across diverse cancer types via the TIMER database.<sup>30</sup> Interestingly, CRIP1 expression was strongly negatively correlated with CD8+T cell infiltration in PDAC compared with other tumours (online supplemental figure 7A–E). In addition, CRIP1 expression exhibited a strong positive correlation with MDSC infiltration in PDAC but not in other tumours (online supplemental figure 7F,G). Based on these results, CRIP1 induces high MDSC infiltration and low T-cell infiltration in PDAC and may have a more significant role in the PDAC immune microenvironment than in other tumours.

### CRIP1-induced CXCL5 and CXCL1 expression contributes to MDSC infiltration in PDAC

To further investigate the relationship between CRIP1 and immune infiltration in PDAC, IHC and immunofluorescence costaining were performed on a tumour microarray to detect MDSC and CD8+T cell infiltration. CRIP1 expression was negatively correlated with CD8+T cell infiltration and positively correlated with MDSC infiltration in PDAC according to the IHC results (figure 3A). The results of immunofluorescence costaining of PDAC tissue further revealed increased numbers of MDSCs and decreased T-cell infiltration in tumour tissues with high CRIP1 expression (figure 3B).

To elucidate the biological functions of CRIP1 in PDAC immune regulation, we assessed the levels of CRIP1 protein in various PDAC cell lines and human pancreatic ductal epithelial cells (figure 3C). CRIP1 was knocked out in CFPAC-1 and SW1990 cell lines with CRISPR–Cas9 technology (figure 3D). CCK-8 and EdU assays showed that CRIP1 had no effect on the growth kinetics of pancreatic cancer cells in vitro (online supplemental figure 8). RNA sequencing was used to reveal the gene expression profiles of CRIP1 knockout SW1990 cells (online supplemental figure 9A). The downregulated genes in the knockout cells were mainly enriched in the term ‘response to cytokine’, and the top DEGs among them were CXCL5 and CXCL1 (figure 3E and F). Real-time PCR and ELISA analysis showed that CRIP1 knockout significantly inhibited the expression of CXCL5 and CXCL1 (figure 3G). In addition, consistent results were observed in the CRIP1-overexpressing group (online supplemental figure 9B). In tumour tissue, the levels of CXCL5 and CXCL1 were higher in PDAC tissues than in normal tissues (online supplemental figure 9C–E). CXCL5 and CXCL1 were abundantly expressed in tumour epithelial cells and were more highly expressed in PDAC tissue with high CRIP1 expression (online supplemental figure 9F,G). Next, we detected CXCL5 and CXCL1 levels in serum and tumour tissue samples from athymic nude mice with subcutaneous xenografts. Lower CXCL5 and CXCL1 expression was detected in tumour tissues from the CRIP1 knockout group, but a significant difference in the serum levels was not observed between the two groups



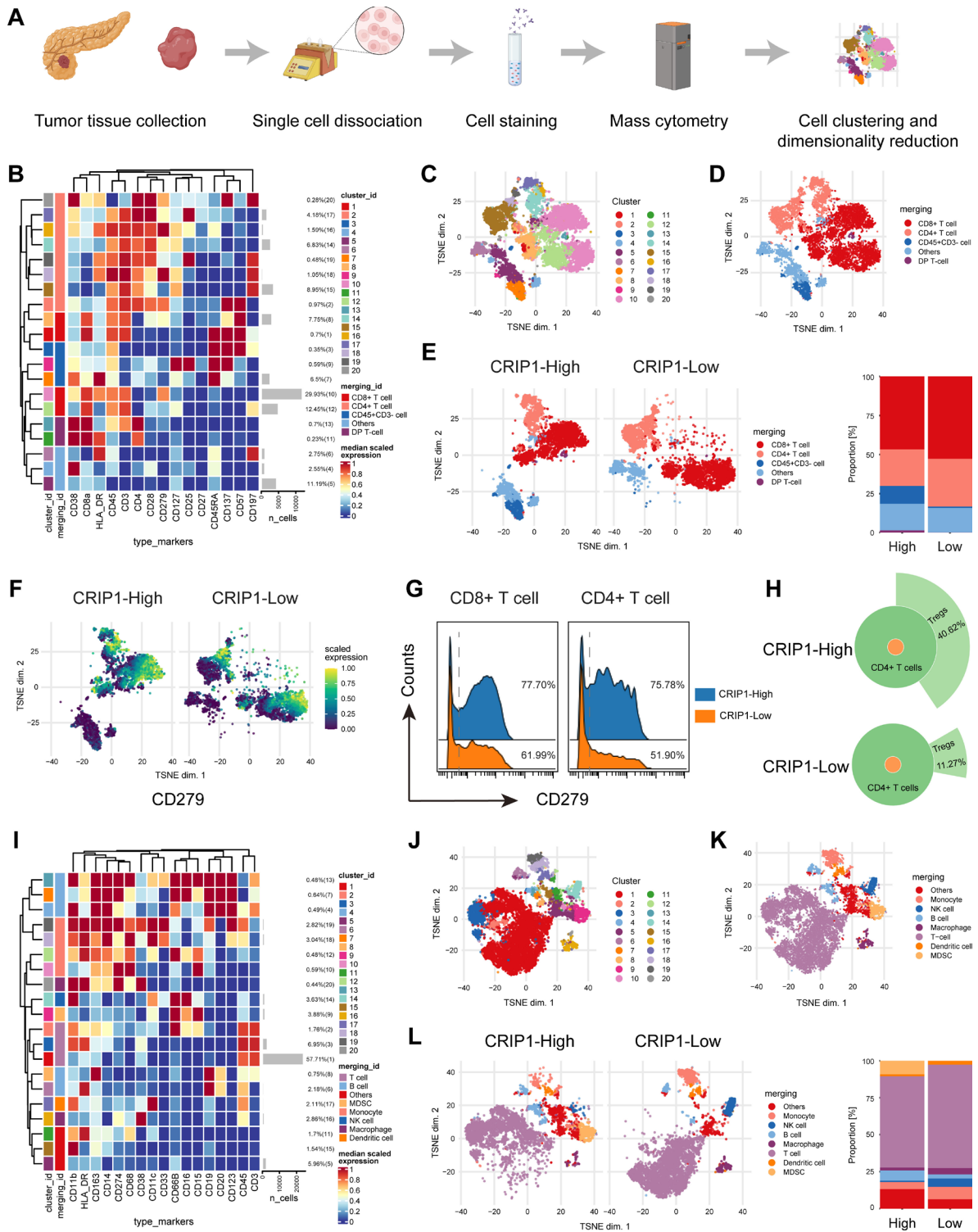


**Figure 2** CRIP1 induces high MDSC infiltration and low T-cell infiltration in the PDAC microenvironment. (A) Schematic illustration of CyTOF data acquisition, including tissue preparation, antibody staining, sample loading, cell clustering and dimensionality reduction. (B) Heatmap of the expression of the 15 markers for the T-cell panel in the 5 cell populations obtained by manual merging of the 20 meta-clusters generated using FlowSOM. (C) FlowSOM defines 20 meta-clusters based on the expression of 15 markers for the T-cell panel in a t-SNE plot. (D) Five cell populations for the T-cell panel obtained by manual merging in a t-SNE plot. (E) The t-SNE plot of T-cell infiltration in the CRIP1 high/low groups. (F) CD279 expression in immune cells in the CRIP1 high/low groups shown in a t-SNE plot. (G) CD279 expression in CD4+ and CD8+ T cells in the CRIP1 high/low groups. (H) Statistical graph of the CyTOF results showed that the proportions of Tregs in CD4+ T cells were increased in the CRIP1 high group. (I) Heatmap of the expression of the 17 markers for the non-T-cell panel in the 8 cell populations obtained by manual merging of the 20 meta-clusters generated using FlowSOM. (J) FlowSOM defines 20 meta-clusters based on the expression of 17 markers for the non-T-cell panel in a t-SNE plot. (K) Eight cell populations for the non-T-cell panel obtained by manual merging in a t-SNE plot. (L) The t-SNE plot of infiltrating cells in the CRIP1 high/low groups. CyTOF, cytometry by time of flight; MDSC, myeloid-derived suppressor cell; PDAC, pancreatic ductal adenocarcinoma; t-SNE, t-distributed stochastic neighbour embedding.

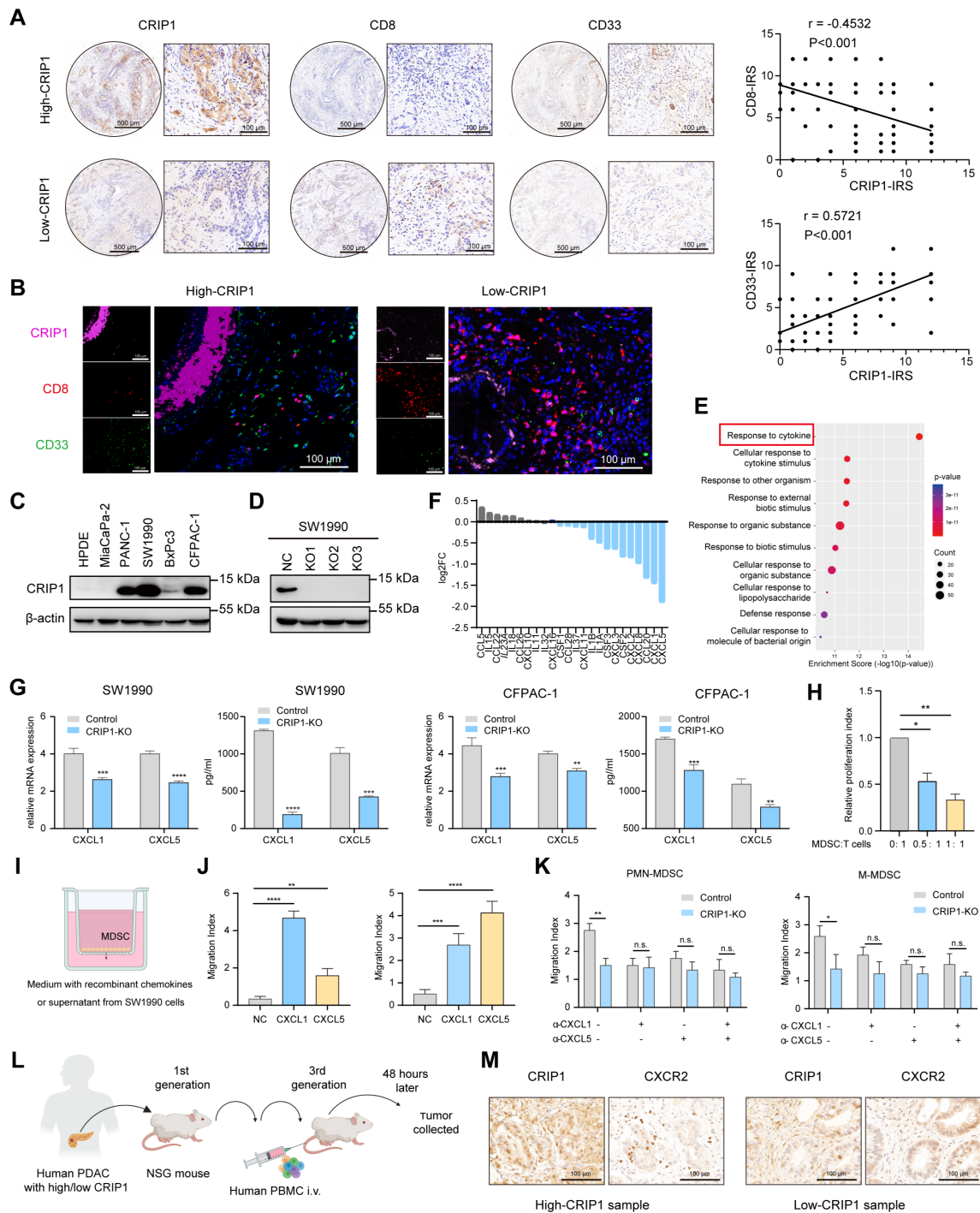


**Figure 3** CRIP1-induced CXCL5 and CXCL1 expression contributes to MDSC infiltration in PDAC. (A) Representative images of IHC staining for CRIP1, CD8 and CD33 in a tissue microarray containing human PDAC samples from FUSCC. Scale bar, 500  $\mu\text{m}$ ; inset scale bar, 100  $\mu\text{m}$ . The correlation between the relative CD33/CD8 IHC score and the relative CRIP1 IHC score ( $n=121$ ). (B) Representative images of immunofluorescence staining for CRIP1 (pink), CD33 (green), CD8 (red) and DAPI (nucleus, blue) in tissue sections from PDAC patients from FUSCC. Scale bar: 100  $\mu\text{m}$ . (C) Western blot analysis of CRIP1 expression in PDAC cell lines and the HPDE cell line;  $\beta$ -actin was used as a control. (D) Western blot analysis of CRIP1 knockout efficiency in SW1990 cells. (E) GO analysis indicated enrichment of the term 'response to cytokine' according to the RNA sequencing data. (F) Histogram of the RNA sequencing-based expression of genes in the 'response to cytokine' list in the SW1990 group normalised to the CRIP1-KO group. (G) Relative expression of the CXCL1 and CXCL5 in PDAC cells was determined using RT-PCR and ELISA. (H) Suppression of T-cell proliferation by MDSCs. (I) Schematic diagram showing the migration of human MDSCs coincubated with recombinant chemokines or culture medium supernatant from PDAC cells. (J) Effects of rCXCL1 and rCXCL5 on the migratory ability of M-MDSCs and PMN-MDSCs. (K) The migratory ability of MDSCs was analysed when PDAC cell culture supernatants were neutralised with  $\alpha$ -CXCL1 and  $\alpha$ -CXCL5 antibodies. (L) Schematic diagram showing the construction of patient-derived xenograft tumour model and human PBMC injection through tail vein. (M) Representative images of IHC staining for CRIP1 and CXCR2 in pdx tumours in 48 hours after the PBMC injection. \* $P < 0.05$ , \*\* $P < 0.01$ , \*\*\* $P < 0.001$ , \*\*\*\* $P < 0.0001$ , Student's  $t$ -test. FUSCC, Fudan University Shanghai Cancer Center; PBMC, peripheral blood mononuclear cell; PDAC, pancreatic ductal adenocarcinoma; PMN-MDSCs, polymorphonuclear-myeloid-derived suppressor cell.

(online supplemental figure 9H). Thus, CRIP1 regulates CXCL1 and CXCL5 expression in pancreatic cancer cells.

According to previous reports, the migration of MDSCs mainly relies on the expression of the chemokine receptors CXCR1/2 and their cognate ligands CXCL1 and CXCL5.<sup>31 32</sup> Next, we evaluated whether these two chemokines were responsible for MDSC migration *in vitro*. We isolated MDSCs from human peripheral blood and confirmed their immunosuppressive ability through a T-cell proliferation assay (figure 3H; online supplemental figure 9I). The results of subsequent chemotaxis assays indicated that culture medium from CFPAC-1 and SW1990 cells increased the migration of MDSCs compared with culture medium from CRIP1-KO cells (figure 3I–K). We also observed that there were more PMN-MDSCs in peripheral blood samples with high CXCL5 expression (online supplemental figure 9J,K). Based on this result, CXCL5 may play an important role in the chemotaxis of MDSCs in PDAC. Using a patient-derived xenograft tumour model and human peripheral blood mononuclear cells injected through the tail vein, we further observed that samples expressing CRIP1 recruited more MDSCs (figure 3L,M). Overall, we conclude that alterations in CXCL5 and CXCL1 levels induced by CRIP1 contribute to MDSC infiltration in PDAC. In summary, these results suggest that CRIP1 plays a significant regulatory role in the formation of an immunosuppressive environment in PDAC by modulating MDSC infiltration.

### CRIP1 induces translocation of p65 protein into nucleus in an importin-dependent manner

To uncover the regulatory mechanism, we performed a coimmunoprecipitation (Co-IP) assay and mass spectrometry (MS) analysis to detect the proteins that bound to CRIP1 (online supplemental figure 10A). NF- $\kappa$ B is a widely reported transcription factor for cytokines and chemokines.<sup>33</sup> p65, a subunit whose nuclear translocation is essential for NF- $\kappa$ B signalling, was pulled down by CRIP1 (figure 4A,B; online supplemental figure 10B). In addition, immunofluorescence staining confirmed the colocalisation of CRIP1 and p65 in PDAC cells (figure 4C). Moreover, importin subunit alpha-7 (importin- $\alpha$ 7) and importin subunit beta-1 (importin- $\beta$ 1) were also detected as CRIP1-binding proteins (figure 4D–G). The nuclear import of cytoplasmic cargos relies on importin- $\alpha$  and soluble transport factors of importin- $\beta$ 1 in the classical pathway.<sup>34</sup> These Co-IP results suggested that CRIP1 might play roles in the translocation of p65 protein into the nucleus. We further discovered that CRIP1 enhanced the nuclear translocation of p65 by performing WB and immunofluorescence assays (figure 4H,I). To clarify whether the change in chemokine expression was caused by the accumulation of p65 in the nucleus, we constructed cell lines with p65 knockout and a mutated nuclear localisation signal (NLS) on p65 to disrupt its nuclear translocation (figure 4J,K; online supplemental figure 10C,D). The results indicated that although CRIP1-induced p65 nuclear translocation increased chemokine expression, this effect disappeared in cells overexpressing p65MutNLS (figure 4L; online supplemental figure 10E). Next, we transfected an importin  $\beta$ 1-siRNA into PDAC cells to knock down importin  $\beta$ 1 expression, and the results showed that p65 nuclear translocation was impaired (figure 4M). CRIP1-induced chemokine expression was also disrupted (figure 4N; online supplemental figure 10F). Thus, p65 nuclear translocation mediated by importin is important for CRIP1-induced CXCL1 and CXCL5 expression. These results suggest that CRIP1-induced p65 nuclear translocation increases chemokine expression in an importin-dependent manner.

### CRIP1 cooperates with p65 to regulate CXCL5 and CXCL1 transcription in PDAC

Next, we demonstrated that CRIP1 increased the activity of the CXCL5 and CXCL1 promoters to upregulate transcription by performing a luciferase reporter assay (figure 5A). We designed 10 pairs of primers that covered all potential binding sites in promoter regions and conducted chromatin immunoprecipitation (ChIP) assays to determine the CRIP1 binding regions in the CXCL5 and CXCL1 promoters (figure 5B). The ChIP-qPCR results indicated that CRIP1 occupied one region in the CXCL1 promoter and two regions in the CXCL5 promoter (figure 5C,D). Furthermore, we confirmed that CRIP1 increased the enrichment of the chromatin activation markers H3K4me and H3K27ac in these binding regions (figure 5E,F). As CRIP1 and p65 were colocalised and functioned in CFPAC-1 and SW1990 cell lines, we deduced that CRIP1 and p65 might interact at the CXCL5 and CXCL1 promoter regions. ChIP assays showed that p65 interacts with the same binding sites in the CXCL5 and CXCL1 promoter regions (figure 5G). ChIP-qPCR assays were performed to assess the interactions of CRIP1 and p65 with chromatin elements in the CXCL5 and CXCL1 promoter regions, and the results showed decreased occupation of the promoter regions by p65 on CRIP1 knockout (figure 5H,I).

As a method to determine the specific binding elements in the CXCL5 and CXCL1 promoters, we mutated the binding sites to establish mutant promoter constructs based on<sup>35</sup> (figure 5J).<sup>35</sup> Subsequent luciferase assays revealed that when the sequences of the binding sites were mutated, the positive effects of CRIP1 and p65 on the luciferase activity of the mutant promoter construct decreased (figure 5K and L). Therefore, CRIP1 enhances the occupation of the promoter regions by p65 and promotes the transcriptional activity of p65.

CFPAC-1 and SW1990 cells overexpressing CRIP1 were treated with the small-molecule NF- $\kappa$ B inhibitor Bay11-7082 to further evaluate the dependence of CRIP1-induced chemokine production on NF- $\kappa$ B. As expected, NF- $\kappa$ B suppression significantly decreased the CXCL5 and CXCL1 mRNA and protein levels in both cell lines (figure 5M and N). Decreased promoter activity of CXCL5 and CXCL1 was also detected when NF- $\kappa$ B was suppressed (online supplemental figure 10G). Moreover, compared with transfection of the p65 vector alone, cotransfection of the CRIP1 and p65 vectors increased CXCL5 and CXCL1 promoter activities (online supplemental figure 10H). These results indicate that CRIP1 promotes the transcription of downstream chemokines through p65.

### CRIP1 promotes *in vivo* tumour growth and induces an immunosuppressive TME

To examine how CRIP1 contributes to tumour progression *in vivo*, we overexpressed CRIP1 in the mouse PDAC cell line Pan02, which showed faint CRIP1 protein expression (online supplemental figure 11A). Moreover, overexpression of CRIP1 did not significantly affect the growth kinetics of Pan02 cells (online supplemental figure 11B). We then confirmed that high levels of CXCL5 and CXCL1 were present in cells with high CRIP1 expression (online supplemental figure 11C). Next, we developed an orthotopic allograft tumour model with Pan02 cell lines in C57BL/6 mice (online supplemental figure 11D). The tumour burden in the CRIP1-overexpressing group was larger than that in the control group (figure 6A–C). The intratumoural CXCL1 and CXCL5 levels in isolated homogenised tumours were markedly higher in CRIP1-overexpressing tumours (figure 6D; online supplemental figure 11E). We next performed



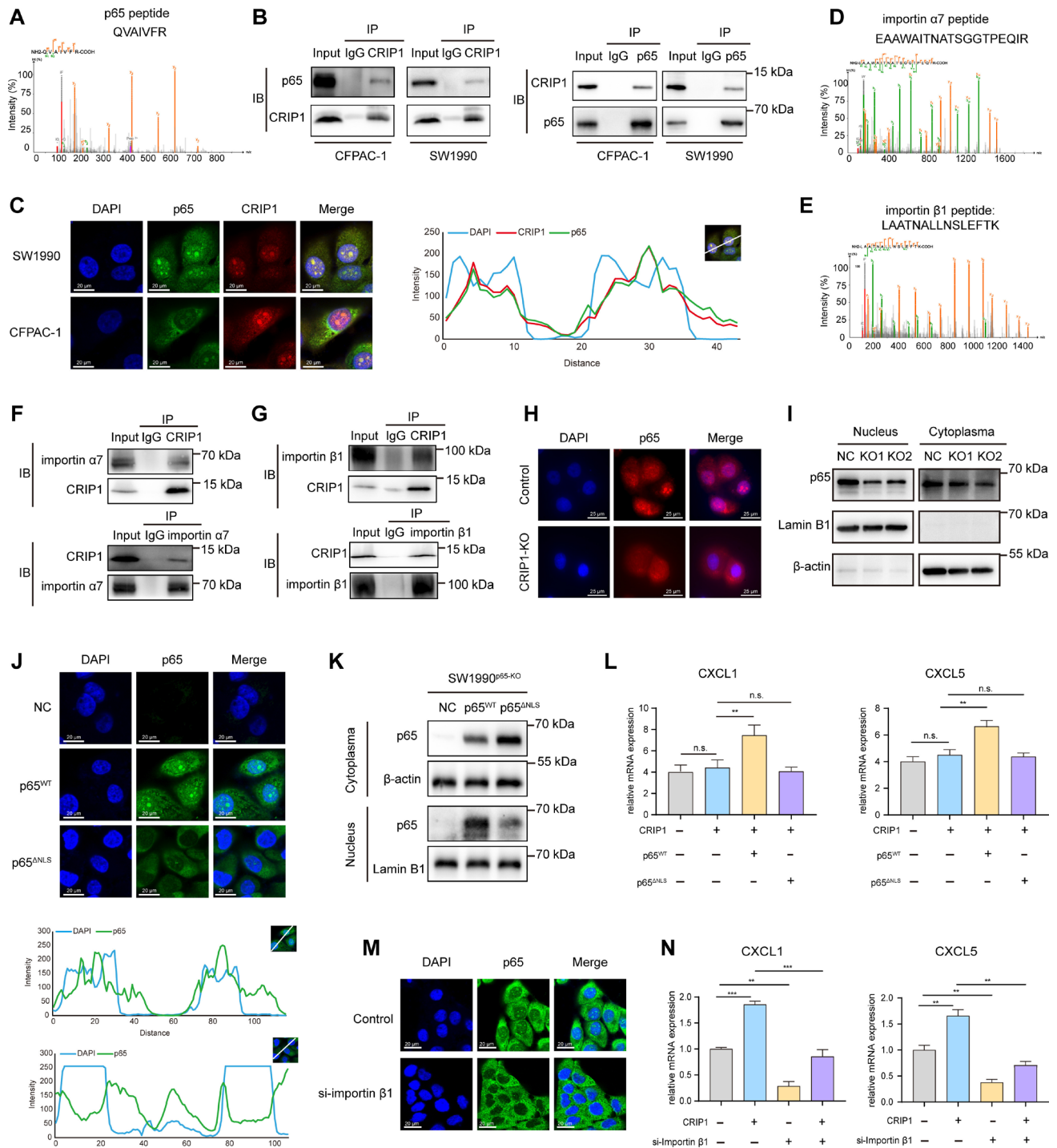


**Figure 4** CRIP1 induces translocation of p65 protein into nucleus in an importin-dependent manner. (A) LC-MS/MS spectrum showing the p65 peptides pulled down by CRIP1. (B) Co-IP of endogenous CRIP1 and p65 in PDAC cells. (C) Representative images of immunofluorescence staining showing the colocalisation of CRIP1 (red) and p65 (green) in PDAC cells. DAPI: blue, nucleus; scale bar: 20  $\mu$ m. Line chart of fluorescence signal positioning analysis. (D, E) LC-MS/MS spectrum showing the peptides of importin- $\alpha$ 7 and importin- $\beta$ 1 pulled down by CRIP1. (F) Co-IP of endogenous CRIP1 and importin- $\alpha$ 7 in PDAC cells. (G) Co-IP of endogenous CRIP1 and importin- $\beta$ 1 in PDAC cells. (H) Representative images of immunofluorescence staining showing the subcellular distribution of p65 (red) in PDAC cells with CRIP1 knockout. DAPI: blue, nucleus; scale bar: 25  $\mu$ m. (I) Immunoblotting of nuclear and cytoplasmic extracts of CRIP1 knockout SW1990 cells. LaminB1 and  $\beta$ -actin were used as nuclear and cytoplasmic controls, respectively. (J, K) The vectors with wild-type p65 (p65<sup>WT</sup>) and a mutation (p65 <sup>$\Delta$ NLS</sup>) that disrupted p65 translocation into the nucleus were transfected into p65 knockout PDAC cells. Immunofluorescence staining of the subcellular distribution of p65 (scale bar, 20  $\mu$ m). Line chart of fluorescence signal positioning analysis. Western blot analysis of nuclear and cytoplasmic protein levels. (L) Relative expression of CXCL1 and CXCL5 in cells transfected with p65<sup>WT</sup> and p65 <sup>$\Delta$ NLS</sup> plasmids. (M) Immunofluorescence staining showing the subcellular distribution of p65 in SW1990 cells with importin- $\beta$ 1 knockdown (scale bar, 20  $\mu$ m). (N) Relative expression of CXCL1 and CXCL5 in cells with importin- $\beta$ 1 knockdown. \* $P$ <0.05, \*\* $P$ <0.01, \*\*\* $P$ <0.001, Student's  $t$ -test. Co-IP, coimmunoprecipitation; LC-MS/MS, liquid chromatography-tandem mass spectrometry; PDAC, pancreatic ductal adenocarcinoma.

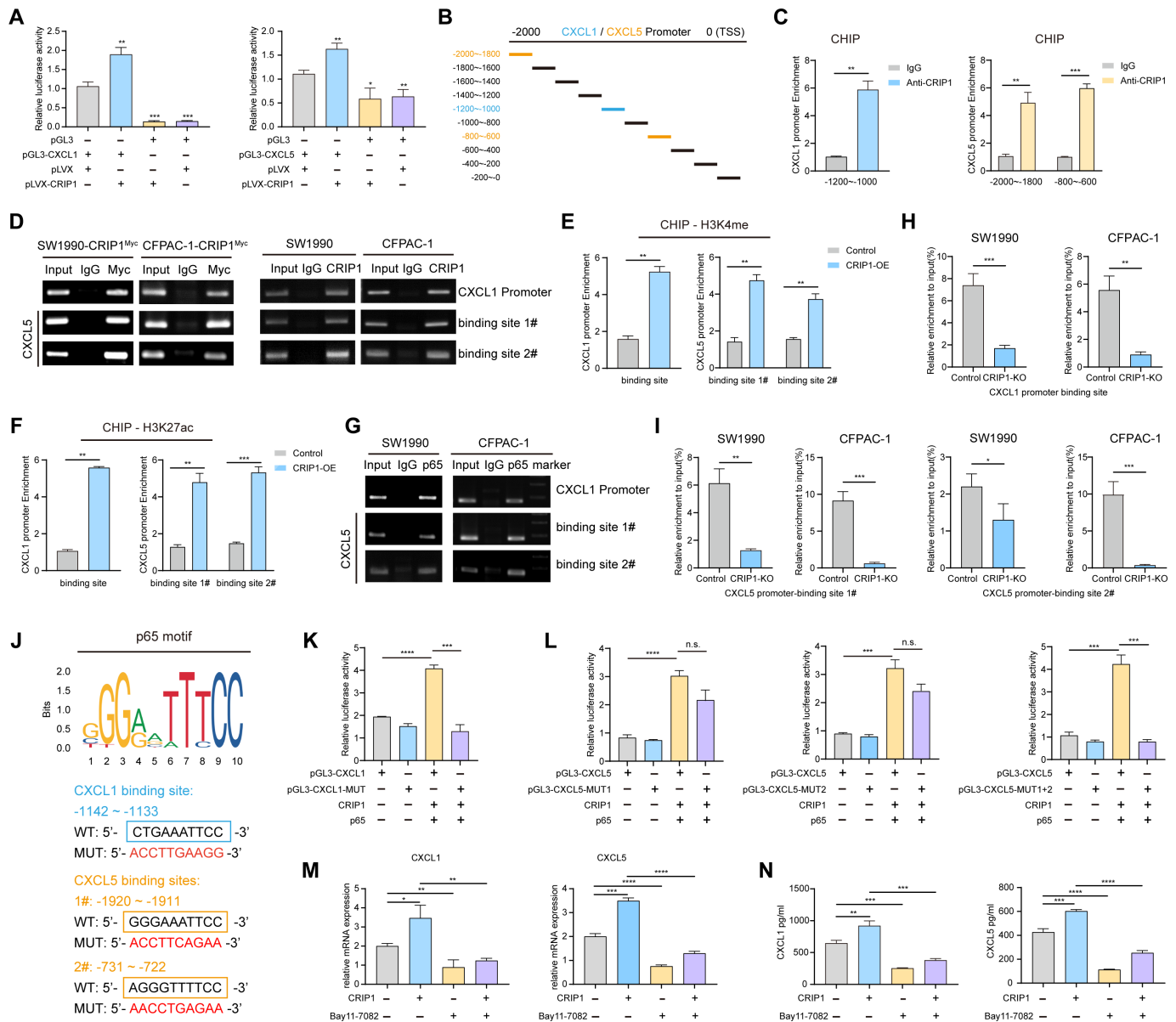


**Figure 5** CRIP1 cooperates with p65 to regulate CXCL5 and CXCL1 transcription in PDAC. (A) The effect of CRIP1 on CXCL5 and CXCL1 promoter activity was examined by performing a dual luciferase reporter assay. (B, C) Quantitative analysis of ChIP assay results indicating the CRIP1 binding regions in the CXCL1 and CXCL5 promoters. (D) Immunoblotting of ChIP assay results showing the binding regions in the CXCL1 and CXCL5 promoters occupied by CRIP1. (E, F) ChIP-qPCR was performed to detect H3K4me and H3K27ac enrichment in the CXCL1 and CXCL5 promoters in PDAC cells overexpressing CRIP1. (G) Immunoblot of ChIP assay results showing that p65 bound the same regions in the CXCL1 and CXCL5 promoters that were occupied by CRIP1. (H, I) ChIP-qPCR indicating that CRIP1 promoted p65 occupation of the CXCL1 and CXCL5 promoters. (J) Schematic representation of the binding sites for p65 in the CXCL1 and CXCL5 promoters. Sequences of the wild-type (WT) and mutated (MUT) binding sites in the promoter regions used in the luciferase reporter constructs. The red characters indicate mutated sequences. (K, L) Dual luciferase reporter assay indicating that CRIP1 and p65 increased the activity of the wild-type CXCL1 and CXCL5 promoters but had no effect on the activity of the mutated promoter. (M, N) RT-PCR and ELISA showing the effect of the NF- $\kappa$ B inhibitor Bay11-7082 (10  $\mu$ M) on CXCL1 and CXCL5 expression in PDAC cells. \* $P$ <0.05, \*\* $P$ <0.01, \*\*\* $P$ <0.001, \*\*\*\* $P$ <0.0001, Student's  $t$ -test. ChIP, chromatin immunoprecipitation; PDAC, pancreatic ductal adenocarcinoma.

a flow cytometry analysis of tumour-infiltrating immune cells collected from tumours (online supplemental figure 11E,G). A substantial increase in the CD11b+Gr1+ population among immune cells, representing MDSCs in mice, was observed in CRIP1-overexpressing tumours (figure 6E). The mRNA expression levels of Arg1 and inducible nitric oxide synthase (iNOS), which are markers of MDSCs, were increased (figure 6F). L-Arginase is depleted by iNOS, and Arg1 is produced by MDSCs, leading to the suppression of T cells.<sup>36</sup> IHC staining showed the same increase in the number of MDSCs in CRIP1-overexpressing

tumours (figure 6G). Flow cytometry analysis confirmed that the populations of CD3+T cells and CD8+T cells were decreased in CRIP1-overexpressing tumours. Although the infiltration of CD4+T cells was not significantly different, the ratio of CD4+T cells to CD3+T cells was obviously increased, which led to a decrease in the CD8+/CD4+ratio (figure 6H,I; online supplemental figure 11H). IHC staining showed the same decrease in CD8+T cells in CRIP1-overexpressing tumours (figure 6J). No significant difference in the T-cell population in the spleen was observed between the two groups (online supplemental figure

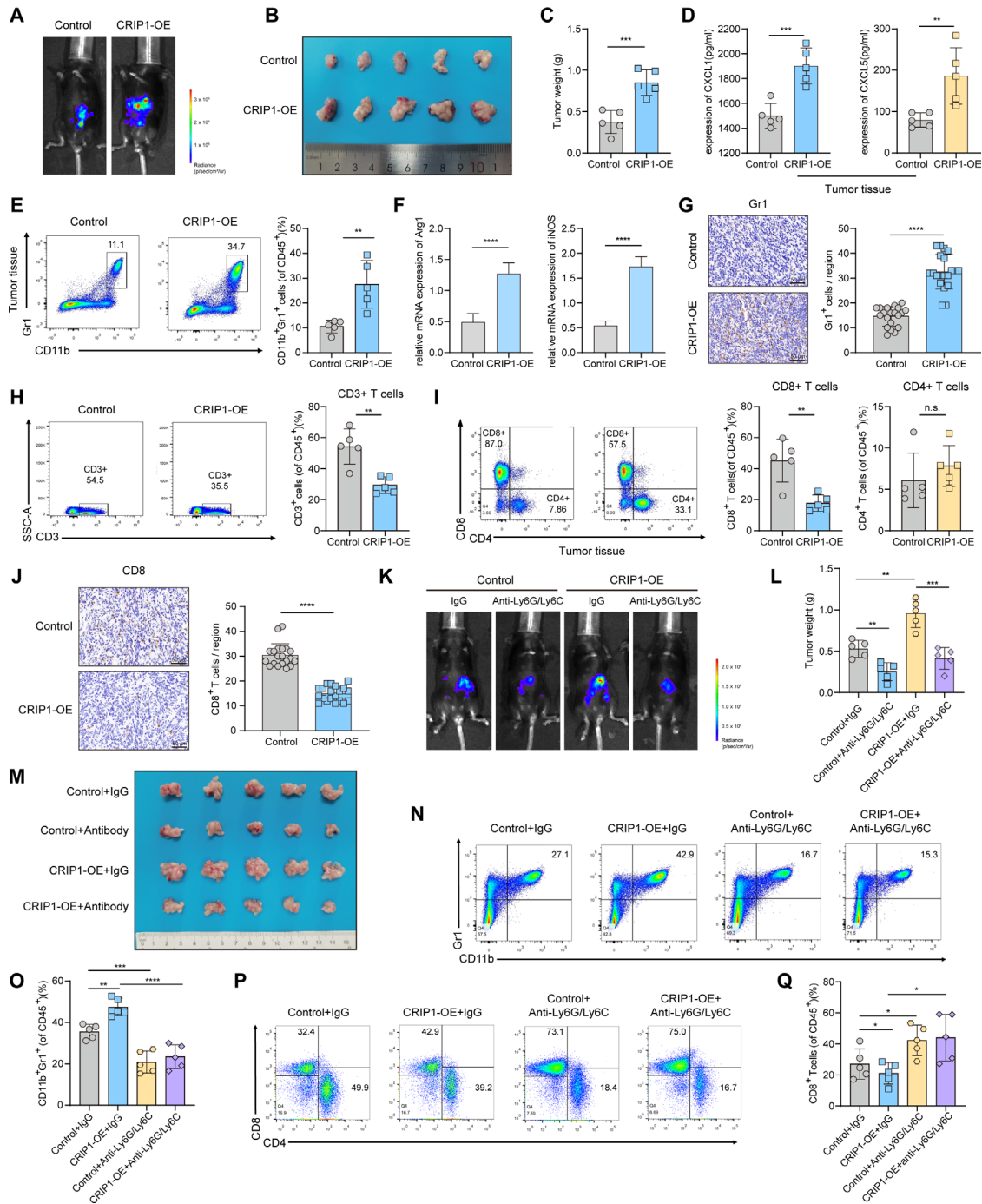


**Figure 6** CRIP1 promotes in vivo tumour growth and induces an immunosuppressive TME dependent on MDSC recruitment. (A) Bioluminescence images of PDAC tumours from the orthotopic allograft tumour model of C57BL/6 mice obtained at the endpoint. The colour scale bar depicts the photon flux emitted from tumours. (B) Image of PDAC tumours in the orthotopic allograft tumour model at the endpoint. (C) Tumour weight data were analysed statistically (n=5). (D) ELISA of CXCL1 and CXCL5 levels in mouse tumour tissues. (E) CD11b<sup>+</sup>Gr1<sup>+</sup> MDSCs in orthotopic allograft tumours from each group were assessed using flow cytometry. Left panel: Representative flow cytometry data showing the proportion of MDSCs in tumour tissues from C57BL/6 mice. The quantification is shown in the right panel. (F) RT-PCR analysis of Arg-1 and iNOS levels in MDSCs from each group. (G) Representative images and quantification of IHC staining for Gr1 in mouse tumour tissues from each group. Scale bar, 50  $\mu$ m. (H, I) Representative flow cytometry data and quantification graph showing the proportion of T cells in tumour tissues from C57BL/6 mice. (J) Representative images and quantification of IHC staining for CD8 in mouse tumour tissues from each group. Scale bar, 50  $\mu$ m. (K) A PDAC orthotopic allograft tumour model was constructed in C57BL/6 mice. Mice were treated with an isotype control or anti-mouse Ly6G/Ly6C (Gr-1) antibody (100  $\mu$ g/mouse i.p.; every 2 days). Bioluminescence images of PDAC tumours from the orthotopic allograft tumour model obtained at the endpoint. (L) Tumour weight data were analysed statistically (n=5). (M) Image of PDAC tumours in the orthotopic allograft tumour model at the endpoint. (N, O) CD11b<sup>+</sup>Gr1<sup>+</sup> MDSCs in tumours from each group were measured using flow cytometry, and the quantification is shown. (P, Q) Representative flow cytometry data showing the proportion of T cells in tumour tissues from C57BL/6 mice. The quantification is shown on the right. \*P < 0.05, \*\*P < 0.01, \*\*\*P < 0.001, \*\*\*\*P < 0.0001, Student's t-test. iNOS, inducible nitric oxide synthase; MDSC, myeloid-derived suppressor cell; PDAC, pancreatic ductal adenocarcinoma; TME, tumour microenvironment.



11I,J). The CD11b+Gr1+ population in immune cells was increased in tumour samples compared with spleen samples, although the CD11b+Gr1+ population in the spleen was not significantly different between the two groups (online supplemental figure 11K,L).

To confirm the role of CRIP1 *in vivo* tumour growth, we isolated tumour cells from KPC (K-Ras<sup>LSL-G12D</sup>; TP53<sup>LSL-R172H</sup>; Pdx-Cre) mouse tumours and cultured them *in vitro*. qPCR and WB analysis showed that the expression of CRIP1 in KPC cells was significantly higher than that in Pan02 cells (online supplemental figure 12A,B). We knocked down CRIP1 in KPC cells, and inhibition of CRIP1 did not significantly affect the growth kinetics of KPC cells (online supplemental figure 12C). An orthotopic allograft tumour model was established in C57BL/6 mice with KPC cells. The tumour burden in the CRIP1-KD group was lower, as expected (online supplemental figure 12D–F). Flow cytometry analysis further showed that the CD8+T cell population was increased and the CD11b+Gr1+ population was decreased in CRIP1-KD tumours (online supplemental figure 12G–J). These results suggest the involvement of both MDSCs and chemokines in eliciting immunosuppression in CRIP1-overexpressing tumours.

### CRIP1-mediated tumour progression depends on the recruitment of MDSCs

We investigated tumour growth in an orthotopic allograft tumour model with MDSC depletion to determine whether CRIP1-facilitated tumour progression depends on MDSCs. Notably, the increased tumour burden induced by CRIP1 overexpression was considerably attenuated in mice that had been treated with anti-Ly6G/Ly6C monoclonal antibodies (figure 6K–M). Treatment with anti-Ly6G/Ly6C monoclonal antibodies was sufficient to decrease the number of CD11b+Gr1+ MDSCs in pancreatic tumours, although this treatment did not completely eliminate MDSCs (figure 6N and O). Simultaneously, the treatment led to an increase in the CD8+T cell population and the CD8+/CD4+ratio (figure 6P and Q; online supplemental figure 13A). Consistent with the flow cytometry analysis, IHC staining showed a decrease in MDSC numbers and an increase in CD8+T cell numbers in tumours from mice treated with anti-Ly6G/Ly6C monoclonal antibodies (online supplemental figure 13B,C). According to these results, the tumour-promoting effects of CRIP1 on PDAC are at least partially mediated by MDSC infiltration in the TME.

### CXCR1/2 inhibitor sensitises anti-PD-L1 blockade therapy in tumour-bearing mice with high CRIP1 expression

CXCR1/2 are the main receptors expressed on MDSCs for CXCL1 and CXCL5, and SX-682 is a potent allosteric inhibitor of CXCR1/2 that blocks MDSC recruitment.<sup>16 17</sup> We investigated tumour growth in a mouse model treated with SX-682 and observed that SX-682 restrained tumour growth in the CRIP1-overexpressing group compared with controls (online supplemental figure 14A,B). Flow cytometry and IHC staining analysis showed that mice treated with SX-682 displayed reductions in MDSC infiltration and an increase in the CD8+T cell population in the CRIP1-overexpressing group (online supplemental figure 14C–G). The mRNA expression levels of Arg-1 and iNOS were decreased in SX-682-treated mice from the CRIP1-overexpressing group (online supplemental figure 14H,I). In summary, blockade of the function of CXCL1/5 by CXCR1/2 inhibitors restrains MDSC trafficking and suppressive functions, facilitating the infiltration of cytotoxic T cells

into tumours, which decreases tumour growth in mice with high CRIP1 expression.

Given the ability of MDSCs to limit the antitumour T-cell response, we then speculated that blocking the CXCL/CXCR axis might improve the efficacy of anti-PD-L1 blockade therapy in PDAC. The combination of anti-PD-L1 therapy and SX-682 significantly inhibited tumour growth and promoted survival compared with that with the control treatment or a single agent alone (figure 7A–C). Flow cytometry analysis revealed a significant increase in the number of T cells in mice treated with the combination of SX-682 and anti-PD-L1 therapy (figure 7D). Importantly, in the combination treatment group, the percentage of CD8+T cells and the CD8+/CD4+ratio was increased compared with those in the groups treated with SX-682 or anti-PD-L1 alone (figure 7E,F). We evaluated biomarkers indicative of CD8+T cell activation in tumours to validate the activation of tumour-infiltrating CD8+T cells. Increased levels of IFN- $\gamma$  and TNF $\alpha$  secreted from activated CD8+T cells were observed when mice were administered the combination treatment. SX-682 or anti-PD-L1 monotherapy only weakly activated CD8+T cells (figure 7G). We then combined anti-PD-L1 therapy and SX-682 in an orthotopic allograft tumour model with KPC cells, which have high endogenous CRIP1 expression. The combination therapy showed significant inhibition of tumour growth and promotion of survival, as expected (online supplemental figure 15A–D). Flow cytometry analysis indicated a significant increase in the number of T cells in mice with combination therapy (online supplemental figure 15E). These results suggest that the CXCR1/2 inhibitor sensitises tumour-bearing mice with high CRIP1 expression to anti-PD-L1 blockade therapy.

We assessed the prognostic value of CRIP1 expression in PDAC by assessing the TCGA and FUSCC RNA cohorts. The results showed that elevated CRIP1 expression was correlated with a poor prognosis for patients with PDAC in both TCGA and FUSCC RNA cohorts (figure 7H,I). IHC staining was performed with a TMA containing 271 patient tissues to explore the prognostic value of the CRIP1 protein level (figure 7J). Patients with high CRIP1 expression showed significantly shorter OS times than those with low CRIP1 expression (figure 7K). The clinical characteristics of the patients in this cohort are presented in online supplemental table 1. Moreover, CRIP1 was identified as an independent prognostic marker of PDAC through Cox regression analyses (table 1). We further explored CRIP1 expression in distinct molecular subtypes based on TCGA datasets. The results showed that CRIP1 had the lowest expression in the exocrine cluster by Collisson subtyping and the lowest expression in the ADEX cluster by Bailey subtyping. No difference in CRIP1 expression was found between the basal and classical subtypes, indicating that CRIP1 expression may be a novel biomarker independent of Moffitt subtypes (online supplemental figure 16A–C). GATA6 loss was a symbol for the basal subcluster, and EZH2 is a histone methyltransferase enhancer that repressed the expression of GATA6. Here, we found no correlation between CRIP1 and GATA6 expression but a high correlation between CRIP1 and EZH2 expression (online supplemental figure 16D,E). KRAS, SMAD4, TP53 and CDKN2A were regarded as four driver genes mediating the genomic events for PDAC.<sup>2</sup> CRIP1 expression was significantly upregulated in the groups with any one driver gene mutation (online supplemental figure 17A–D). This is also consistent with the results that CRIP1 is highly expressed in KPC cells in online supplemental figure 12. Furthermore, we found that the expression of CRIP1 in patients with both KRAS and SMAD4 mutations was significantly upregulated compared with that in patients with only KRAS or SMAD4

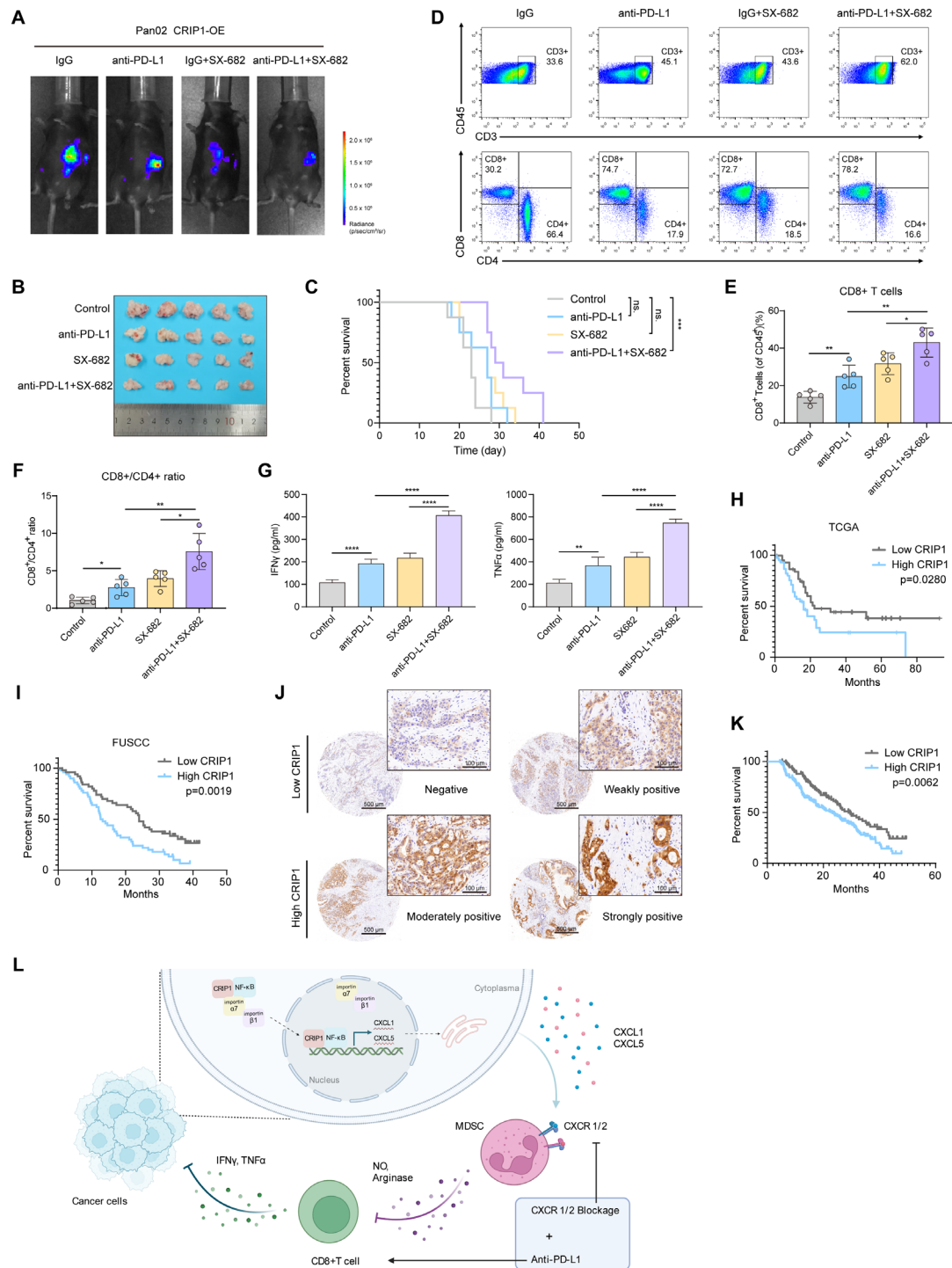


**Figure 7** CXCR1/2 inhibitor sensitises tumour-bearing mice with high CRIP1 expression to anti-PD-L1 blockade therapy. (A) A PDAC orthotopic allograft tumour model was constructed with CRIP1-OE Pan02 cells ( $5 \times 10^5$  cells) in C57BL/6 mice. Mice were treated with SX-682 (50 mg/kg; orally; twice a day) and anti-PD-L1 (200  $\mu$ g/mouse; i.p.; twice a week) starting on day 5 post-tumour cell inoculation. Bioluminescence images of PDAC tumours from the orthotopic allograft tumour model obtained at the endpoint. (B) Image of PDAC tumours in the orthotopic allograft tumour model at the endpoint. (C) Kaplan-Meier analysis (log-rank test) of mice in each treatment group ( $n=8$ ).  $***P < 0.001$ . (D–F) CD3<sup>+</sup>, CD4<sup>+</sup> and CD8<sup>+</sup> T cells in orthotopic allograft tumours from each group were measured using flow cytometry. Representative flow cytometry data showing the proportion of T cells in tumour tissues from C57BL/6 mice.  $*P < 0.05$ ,  $**P < 0.01$ , Student's *t*-test. (G) IFN- $\gamma$  and TNF $\alpha$  levels in each group of orthotopic allograft tumours were analysed using ELISA.  $**P < 0.01$ ,  $****P < 0.0001$ , Student's *t*-test. (H) Kaplan-Meier analysis (log-rank test) of the overall survival of patients with PDAC based on CRIP1 expression. Data were derived from the TCGA cohort (cut-off: quartile). (I) Kaplan-Meier analysis (log-rank test) of the overall survival of patients with PDAC from FUSCC based on CRIP1 mRNA expression ( $n=100$ ). (J) Representative images of IHC staining for CRIP1 in a human PDAC tissue microarray containing samples from patients at FUSCC ( $n=271$ ). Scale bar, 500  $\mu$ m; inset scale bar, 100  $\mu$ m. (K) Kaplan-Meier analysis (log-rank test) of the overall survival of patients with PDAC from FUSCC based on the CRIP1 IHC staining score. (L) Schematic diagram depicting the microenvironment induced by the CXCR1/2 inhibitor and PD-L1 blockade in patients with PDAC with high CRIP1 expression. FUSCC, Fudan University Shanghai Cancer Center; PDAC, pancreatic ductal adenocarcinoma; TCGA, The Cancer Genome Atlas.

**Table 1** Univariate and multivariate Cox regression of overall survival for PDAC patients in FUSCC

Characteristics	Univariate			Multivariate		
	HR	95% CI	P value	HR	95% CI	P value
Age						
≥65 years	1.076	0.781 to 1.483	0.654			
<65 years						
Gender						
Male	1.242	0.910 to 1.694	0.172			
Female						
TNM stage						
III	2.072	1.402 to 3.062	<0.001	1.791	1.174 to 2.733	0.007
I–II						
Histological grade						
Low	1.353	0.990 to 1.850	0.058	1.456	1.062 to 1.996	0.020
Moderate/high						
Tumour size						
>4 cm	1.430	1.021 to 2.003	0.037	1.373	0.972 to 1.940	0.072
≤4 cm						
Lymph node status						
Positive	1.446	1.054 to 1.985	0.022	1.118	0.788 to 1.586	0.532
Negative						
Vascular invasion						
Positive	1.460	1.073 to 1.985	0.016	1.404	1.024 to 1.924	0.035
Negative						
CA19–9 ≥37 U/mL						
Yes	1.670	1.085 to 2.571	0.020	1.453	0.932 to 2.264	0.099
No						
CRIP1 expression						
High	1.554	1.130 to 2.137	0.007	1.413	1.022 to 1.952	0.036
Low						

FUSCC, Fudan University Shanghai Cancer Center; PDAC, pancreatic ductal adenocarcinoma; TNM, tumour node metastasis.

mutation (online supplemental figure 17E). The above results suggest that in patients with co-occurring KRAS and SMAD4 mutations, CRIP1 is highly expressed and fosters a suppressive tumour immune microenvironment (TIME) by means of MDSC recruitment.

Based on these results, we generated a schematic diagram depicting the microenvironment induced by CXCR1/2 and PD-L1 blockade in PDAC with high CRIP1 expression (figure 7L). CRIP1 facilitates importin-dependent p65 nuclear translocation and increases the occupation of the CXCL1 and CXCL5 promoters by p65. CRIP1-induced chemokine production facilitates the chemotactic migration of MDSCs into the PDAC microenvironment, which increases the production of immunosuppressive cytokines and restrains activated CD8+T cells. Blocking the CRIP1/CXCL/CXCR1/2 pathway suppresses MDSC recruitment and subsequently activates CD8+T cells. Combining anti-PD-L1 therapy and CXCR1/2 inhibition elicits potent antitumour activity and increases treatment efficacy in PDAC with high CRIP1 expression.

## DISCUSSION

CRIP1 is aberrantly expressed in various tumour types and appears to have tumour type-specific properties based on limited reports.<sup>37–39</sup> However, the role of CRIP1 in PDAC has rarely been studied. Chen *et al* suggested the participation of CRIP1 in the evolution of fibroblasts in PDAC progression through bioinformatic analysis.<sup>40</sup> However, there was neither bioinformatic analysis nor experiments to further explore the specific

mechanism of CRIP1 in PDAC in this study. Here, we integrated two large open scRNA-seq datasets of PDAC and found that CRIP1 is significantly upregulated in ductal cells isolated from PDAC, which is consistent with the results from bulk RNA-seq, qPCR and IHC reported in our manuscript.

Although the detailed mechanism underlying the effects of elevated CRIP1 expression in pancreatic tumour cells is currently unclear, strategies targeting CRIP1 may be effective in the clinic, as high CRIP1 expression predicts a poor prognosis for patients with PDAC and facilitates the formation of an immunosuppressive microenvironment. The role of CRIP1 in tumour immunity has not been reported, but a previous study showed that CRIP1 was detected in immune cells present in rat tissues and was involved in host defence.<sup>41</sup> This result suggests that CRIP1 may directly affect the differentiation and function of immune cells. Thus, the role of CRIP1 in inflammation and immune infiltration is an issue that warrants further investigation. We observed that CRIP1 expression was elevated in PDAC and inversely correlated with antitumour immune signatures. However, CRIP1 expression is positively correlated with the levels of antitumour immune cells in some other cancers, such as lung squamous cell carcinoma and HPV-positive head and neck squamous cell carcinoma. Therefore, CRIP1-mediated immunoregulation operates differently in various cancers. More extensive studies are needed to explain the mechanism underlying this phenomenon.

CRIP1 can induce the expression of other cytokine/chemokine genes, as the RNA sequencing results showed, and we



cannot completely exclude the possibility that these cytokines/chemokines also modulate immune and/or non-immune components of the TME and promote tumour growth. Furthermore, the possibility that CRIP1 also affects other aspects of PMN-MDSCs, such as their longevity, immunosuppressive potential or differentiation, cannot be excluded. We found that CRIP1 induces CXCL family chemokine expression in tumour cells by promoting the transcriptional function of NF- $\kappa$ B. NF- $\kappa$ B is a widely reported transcription factor for cytokines and chemokines and is also a classic potential target in tumour therapy.<sup>42</sup> Gao *et al* also observed that the CRIP1-high group in acute myeloid leukaemia had an enrichment of TNF $\alpha$  signalling via the NF $\kappa$ B pathway, which supported our conclusion.<sup>43</sup> However, this study involves bioinformatics analysis of a haematological malignancy without any experiments to verify the conclusions. Here, we performed a deep mechanistic exploration and found that CRIP1 binds to p65 and facilitates its nuclear translocation, increasing the occupation of the CXCL1 and CXCL5 promoters by p65.

CRIP1 contributes to PDAC tumour growth in an MDSC-dependent manner *in vivo*. Inhibition of CXCR1/2 prevents MDSC recruitment through CXCL1 and CXCL5, subsequently activating CD8+T cells. Inhibitors of CXCR1 and CXCR2 have been investigated in some clinical trials to treat malignant tumours. However, the combination of a CXCR1/2 inhibitor with paclitaxel in patients with metastatic breast cancer did not provide compelling evidence of augmented clinical activity.<sup>44 45</sup> The combination of MDSC inhibition and ICB therapy resulted in a modest tumour response in short-term mouse experiments.<sup>46</sup> At present, SX-682 combined with PD1 inhibitors has been studied in a phase I clinical trial in PDAC, but the results have not yet been disclosed, and the therapeutic efficacy remains uncertain. In addition to exploring how to improve the tumour microenvironment, it is also critical to select patients who can benefit from immunotherapy for precise treatment and to determine which combination treatments are most suitable for different groups of people. In our study, SX-682 restrained tumour growth in the CRIP1-overexpressing group but had no significant effects on the tumour burden in the normal tumour-bearing group. Based on the efficacies of various immunotherapies in PDAC, we speculate that a significant number of patients will not respond well to this combination with SX-682, as both cancer cells and the TME in PDAC exhibit substantial heterogeneity. Here, we provide an accurate analysis and prediction of the population that may benefit from this treatment and provide data supporting the potential effectiveness of this combination.

We identified two DEGs in this study, CRIP1 and S100A6. S100A6 is widely studied in PDAC progression, and reports on S100A6 have mainly focused on its effect on tumour cell invasion and proliferation. Although there are few studies on the TIME, S100A6 has been reported to be associated with immune infiltration in other diseases.<sup>47</sup> Therefore, we speculate that S100A6 may have a certain synergistic effect with CRIP1 in the TIME of PDAC. In addition, according to reports, both CRIP1 and S100A6 play certain functions in fibroblasts. Here, we performed CytoTRACE and found that CRIP1 was expressed mostly in stellate cells instead of fibroblasts, while S100A6 was distributed in both fibroblasts and stellate cells. Both CRIP1 and S100A6 were upregulated in more differentiated stellates suggested their participation in the evolution of fibroblasts in PDAC. Here, we speculate that CRIP1 and S100A6 might also play a synergistic role in the fibroblast differentiation potential in PDAC. However, further mechanistic experiments are needed to confirm whether CRIP1 and S100A6 cooperate in the progression of PDAC. We did not conduct experiments in the current

study to further explore this issue, as it is irrelevant to the main content of our study. However, this topic about fibroblasts in PDAC is important and interesting, and we will focus on it in future research.

#### Author affiliations

<sup>1</sup>Department of Pancreatic Surgery, Fudan University Shanghai Cancer Center, Shanghai, China

<sup>2</sup>Department of Oncology, Shanghai Medical College of Fudan University, Shanghai, China

<sup>3</sup>Shanghai Pancreatic Cancer Institute, Shanghai, China

<sup>4</sup>Pancreatic Cancer Institute, Fudan University, Shanghai, China

<sup>5</sup>Department of Pancreatic and Hepatobiliary Surgery, The Affiliated Hospital of Qingdao University, Qingdao, China

<sup>6</sup>Key Laboratory of Growth Regulation and Translational Research of Zhejiang Province, School of Life Sciences, Westlake University, Hangzhou, China

<sup>7</sup>Department of General Surgery, Zhejiang University, Hangzhou, China

**Contributors** XL, RT and JX performed the experiments, manuscript preparation and statistical analysis. XL and RT contributed to the bioinformatics analysis. ZT, CL, YL and JH contributed to the *in vitro* experiments. XL, RT, QM and YZ contributed to the *in vivo* experiments. JL, BZ and WW contributed to the collection of clinical specimens and provided clinical pathology evaluations. XL and JX analysed and interpreted the results of the study. SS and XY conceived, designed and supervised the study and provided a critical review of the manuscript. XL and SS are responsible for the overall content as the guarantor.

**Funding** This study was jointly supported by the National Natural Science Foundation of China (U21A20374), Shanghai Municipal Science and Technology Major Project (21JC1401500), Scientific Innovation Project of Shanghai Education Committee (2019-01-07-00-07-E00057), Clinical Research Plan of Shanghai Hospital Development Center (SHDC2020CR1006A) and Xuhui District Artificial Intelligence Medical Hospital Cooperation Project (2021-011).

**Competing interests** None declared.

**Patient and public involvement** Patients and/or the public were not involved in the design, or conduct, or reporting, or dissemination plans of this research.

**Patient consent for publication** Not applicable.

**Ethics approval** This study involves human participants and this study was approved by the Institutional Research Ethics Committee of FUSCC, and written informed consent was obtained from all patients. 050432-4-1911D. Participants gave informed consent to participate in the study before taking part.

**Provenance and peer review** Not commissioned; externally peer reviewed.

**Data availability statement** All data relevant to the study are included in the article or uploaded as online supplemental information.

**Supplemental material** This content has been supplied by the author(s). It has not been vetted by BMJ Publishing Group Limited (BMJ) and may not have been peer-reviewed. Any opinions or recommendations discussed are solely those of the author(s) and are not endorsed by BMJ. BMJ disclaims all liability and responsibility arising from any reliance placed on the content. Where the content includes any translated material, BMJ does not warrant the accuracy and reliability of the translations (including but not limited to local regulations, clinical guidelines, terminology, drug names and drug dosages), and is not responsible for any error and/or omissions arising from translation and adaptation or otherwise.

**Open access** This is an open access article distributed in accordance with the Creative Commons Attribution Non Commercial (CC BY-NC 4.0) license, which permits others to distribute, remix, adapt, build upon this work non-commercially, and license their derivative works on different terms, provided the original work is properly cited, appropriate credit is given, any changes made indicated, and the use is non-commercial. See: <http://creativecommons.org/licenses/by-nc/4.0/>.

#### ORCID iD

Si Shi <http://orcid.org/0000-0002-6652-0629>

#### REFERENCES

- 1 Siegel RL, Miller KD, Fuchs HE, *et al*. Cancer statistics, 2021. *CA Cancer J Clin* 2021;71:7–33.
- 2 Mizrahi JD, Surana R, Valle JW, *et al*. Pancreatic cancer. *The Lancet* 2020;395:2008–20.
- 3 Conroy T, Hammel P, Hebbar M, *et al*. FOLFIRINOX or Gemcitabine as adjuvant therapy for Pancreatic cancer. *N Engl J Med* 2018;379:2395–406.
- 4 Korman AJ, Garrett-Thomson SC, Lonberg N. The foundations of immune Checkpoint blockade and the Ipilimumab approval Decennial. *Nat Rev Drug Discov* 2022;21:163:509–28..

- 5 Kraehenbuehl L, Weng C-H, Eghbali S, et al. Enhancing Immunotherapy in cancer by targeting emerging immunomodulatory pathways. *Nat Rev Clin Oncol* 2022;19:37–50.
- 6 Eggermont AMM, Chiarion-Sileni V, Grob J-J, et al. Prolonged survival in stage III Melanoma with Ipilimumab adjuvant therapy. *N Engl J Med* 2016;375:1845–55.
- 7 Reck M, Rodríguez-Abreu D, Robinson AG, et al. Pembrolizumab versus chemotherapy for PD-L1-positive non-small-cell lung cancer. *N Engl J Med* 2016;375:1823–33.
- 8 O'Reilly EM, Oh D-Y, Dhani N, et al. Durvalumab with or without Tremelimumab for patients with metastatic Pancreatic Ductal adenocarcinoma: A phase 2 randomized clinical trial. *JAMA Oncol* 2019;5:1431–8.
- 9 Wood LD, Canto MI, Jaffee EM, et al. Pancreatic cancer: pathogenesis, screening, diagnosis and treatment. *Gastroenterology* 2022;163:386–402.
- 10 Ho WJ, Jaffee EM, Zheng L. The tumour Microenvironment in Pancreatic cancer - clinical challenges and opportunities. *Nat Rev Clin Oncol* 2020;17:527–40.
- 11 Binnewies M, Roberts EW, Kersten K, et al. Understanding the tumor immune Microenvironment (TIME) for effective therapy. *Nat Med* 2018;24:541–50.
- 12 Veglia F, Perego M, Gabrilovich D. Myeloid-derived Suppressor cells coming of age. *Nat Immunol* 2018;19:108–19.
- 13 Hegde S, Leader AM, Merad M. MDSC: markers, development, States, and Unaddressed complexity. *Immunity* 2021;54:875–84.
- 14 Rodriguez PC, Hernandez CP, Quiceno D, et al. Arginase 1 in myeloid Suppressor cells is induced by COX-2 in lung carcinoma. *J Exp Med* 2005;202:931–9.
- 15 Mao Y, Poschke I, Wennerberg E, et al. Melanoma-educated Cd14+ cells acquire a myeloid-derived Suppressor cell phenotype through COX-2-dependent mechanisms. *Cancer Res* 2013;73:3877–87.
- 16 Nagarsheth N, Wicha MS, Zou W. Chemokines in the cancer Microenvironment and their relevance in cancer Immunotherapy. *Nat Rev Immunol* 2017;17:559–72.
- 17 Nywening TM, Belt BA, Cullinan DR, et al. Targeting both tumour-associated Cxcr2+ neutrophils and Ccr2+ Macrophages disrupts myeloid recruitment and improves chemotherapeutic responses in Pancreatic Ductal adenocarcinoma. *Gut* 2018;67:1112–23.
- 18 Feig C, Jones JO, Kraman M, et al. Targeting Cxcl12 from FAP-expressing carcinoma-associated fibroblasts Synergizes with anti-PD-L1 Immunotherapy in Pancreatic cancer. *Proc Natl Acad Sci U S A* 2013;110:20212–7.
- 19 Liu X, Xu J, Zhang B, et al. The reciprocal regulation between host tissue and immune cells in Pancreatic Ductal adenocarcinoma: new insights and therapeutic implications. *Mol Cancer* 2019;18:184.
- 20 Anderson KG, Stromnes IM, Greenberg PD. Obstacles posed by the tumor Microenvironment to T cell activity: A case for synergistic therapies. *Cancer Cell* 2017;31:311–25.
- 21 Balachandran VP, Beatty GL, Dougan SK. Broadening the impact of Immunotherapy to Pancreatic cancer: challenges and opportunities. *Gastroenterology* 2019;156:2056–72.
- 22 Dias Carvalho P, Guimarães CF, Cardoso AP, et al. KRAS Oncogenic signaling extends beyond cancer cells to Orchestrate the Microenvironment. *Cancer Res* 2018;78:7–14.
- 23 Li J, Byrne KT, Yan F, et al. Tumor cell-intrinsic factors underlie heterogeneity of immune cell infiltration and response to Immunotherapy. *Immunity* 2018;49:178–93.
- 24 Bayne LJ, Beatty GL, Jhala N, et al. Tumor-derived granulocyte-macrophage colony-stimulating factor regulates myeloid inflammation and T cell immunity in Pancreatic cancer. *Cancer Cell* 2012;21:822–35.
- 25 Chan-Seng-Yue M, Kim JC, Wilson GW, et al. Author correction: transcription phenotypes of Pancreatic cancer are driven by Genomic events during tumor evolution. *Nat Genet* 2020;52:463.
- 26 Hempe JM, Cousins RJ. Cysteine-rich intestinal protein binds zinc during Transmucosal zinc transport. *Proc Natl Acad Sci U S A* 1991;88:9671–4.
- 27 Wang Q, Williamson M, Bott S, et al. Hypomethylation of Wnt5A, Crip1 and S100P in prostate cancer. *Oncogene* 2007;26:6560–5.
- 28 Li H-G, Zhao L-H, Zhang Z-H, et al. The impact of Cysteine-rich intestinal protein 1 (Crip1) on thyroid carcinoma. *Cell Physiol Biochem* 2017;43:2037–46.
- 29 Schapiro D, Jackson HW, Raghuraman S, et al. histoCAT: analysis of cell phenotypes and interactions in Multiplex image Cytometry data. *Nat Methods* 2017;14:873–6.
- 30 Li T, Fu J, Zeng Z, et al. Timer2.0 for analysis of tumor-infiltrating immune cells. *Nucleic Acids Res* 2020;48:W509–14.
- 31 Ozga AJ, Chow MT, Luster AD. Chemokines and the immune response to cancer. *Immunity* 2021;54:859–74.
- 32 Chao T, Furth EE, Vonderheide RH. Cxcr2-dependent accumulation of tumor-associated neutrophils regulates T-cell immunity in Pancreatic Ductal adenocarcinoma. *Cancer Immunol Res* 2016;4:968–82.
- 33 Taniguchi K, Karin M. NF-kappaB, inflammation, immunity and cancer: coming of age. *Nat Rev Immunol* 2018;18:309–24.
- 34 Lott K, Cingolani G. The Importin beta binding domain as a master regulator of Nucleocytoplasmic transport. *Biochim Biophys Acta* 2011;1813:1578–92.
- 35 Castro-Mondragon JA, Riudavets-Puig R, Rauluseviute I, et al. JASPAR 2022: the 9th release of the open-access database of transcription factor binding profiles. *Nucleic Acids Res* 2022;50:D165–73.
- 36 Aarts CEM, Hiemstra IH, Béguin EP, et al. Activated neutrophils exert myeloid-derived Suppressor cell activity damaging T cells beyond repair. *Blood Adv* 2019;3:3562–74.
- 37 Ludyga N, Englert S, Pflieger K, et al. The impact of Cysteine-rich intestinal protein 1 (Crip1) in human breast cancer. *Mol Cancer* 2013;12:28.
- 38 Zhang L, Zhou R, Zhang W, et al. Cysteine-rich intestinal protein 1 suppresses apoptosis and Chemosensitivity to 5-fluorouracil in colorectal cancer through Ubiquitin-mediated Fas degradation. *J Exp Clin Cancer Res* 2019;38:120.
- 39 Sun H, Zhou R, Zheng Y, et al. Crip1 cooperates with Brca2 to drive the nuclear enrichment of Rad51 and to facilitate Homologous repair upon DNA damage induced by chemotherapy. *Oncogene* 2021;40:5342–55.
- 40 Chen K, Wang Q, Li M, et al. Single-cell RNA-Seq reveals dynamic change in tumor Microenvironment during Pancreatic Ductal adenocarcinoma malignant progression. *EBioMedicine* 2021;66:103315.
- 41 Hallquist NA, Khoo C, Cousins RJ. Lipopolysaccharide regulates Cysteine-rich intestinal protein, a zinc-finger protein, in immune cells and plasma. *J Leukoc Biol* 1996;59:172–7.
- 42 Sun SC. The non-Canonical NF-kappaB pathway in immunity and inflammation. *Nat Rev Immunol* 2017;17:545–58.
- 43 Gao Y, Li J-Y, Mao J-Y, et al. Comprehensive analysis of Crip1 expression in acute myeloid leukemia. *Front Genet* 2022;13:13.
- 44 Schott AF, Goldstein LJ, Cristofanilli M, et al. Phase IB pilot study to evaluate Reparixin in combination with weekly paclitaxel in patients with HER-2-negative metastatic breast cancer. *Clin Cancer Res* 2017;23:5358–65.
- 45 Goldstein LJ, Mansutti M, Levy C, et al. A randomized, placebo-controlled phase 2 study of paclitaxel in combination with Reparixin compared to paclitaxel alone as front-line therapy for metastatic triple-negative breast cancer (fRida). *Breast Cancer Res Treat* 2021;190:265–75.
- 46 Kim IS, Gao Y, Welte T, et al. Immuno-Subtyping of breast cancer reveals distinct myeloid cell profiles and Immunotherapy resistance mechanisms. *Nat Cell Biol* 2019;21:1113–26.
- 47 Tong H, Wang L, Zhang K, et al. Correction to: S100A6 activates Kupffer cells via the P-P38 and P-JNK pathways to induce inflammation, mononuclear/macrophage infiltration sterile liver injury in mice. *Inflammation* 2023;46:555.